American Journal of Science, Engineering and Technology
2023; 8(2): 71-80
http://www.sciencepublishinggroup.com/j/ajset
doi: 10.11648/j.ajset.20230802.11
ISSN: 2578-8345 (Print); ISSN: 2578-8353 (Online)

Optimizing the Ceramic Slurry Formulation and Process Conditions for DSW Printing

Zhining Xu[1], Hairong Zhang[1], Ben Yao[1], Jianan Liu[1], Liang Yang[1], Jianping Shang[1], Jingyuan Fan[2], Lizhi Ouyang[3], Hua-Jun Shawn Fan[1, *]

[1]College of Chemical Engineering, Sichuan University of Science and Engineering, Zigong, China

[2]Carnegie Vanguard High School, Houston, USA

[3]Department of Physics and Mathematics, Tennessee State University, Nashville, USA

Email address:

fan27713@yahoo.com (Hua-Jun Shawn Fan)

[*]Corresponding author

To cite this article:

Zhining Xu, Hairong Zhang, Ben Yao, Jianan Liu, Liang Yang, Jianping Shang, Jingyuan Fan, Lizhi Ouyang, Hua-Jun Shawn Fan. Optimizing the Ceramic Slurry Formulation and Process Conditions for DSW Printing. *American Journal of Science, Engineering and Technology*. Vol. 8, No. 2, 2023, pp. 71-80. doi: 10.11648/j.ajset.20230802.11

Received: March 8, 2023; **Accepted**: March 27, 2023; **Published**: April 15, 2023

Abstract: An 3D printing is a popular additive manufacturing tool that attracts attention from many sectors and direct slurry writing (DSW) printing is a suitable technique for creating functional ceramic material. This study investigates the suitable formula with various additives and binders and the process conditions that influence DSW printing quality. To combine the unique properties of PVP and PEG binders and attapulgite, various ceramic slurry formulas of attapulgite and TiO_2 mixture were prepared for direct slurry writing (DSW) printing. Establishing both qualitative and quantitative assessments on the rheological outcomes, the ceramic slurry formula, printing parameter, drying, and sintering conditions, and the binder ratio for ceramic slurries was optimized. The results showed that the most optimal ratio for ceramic slurries is with 10% PVP or 5% PEG binder and the optimal attapulgite:TiO_2 ratio is 1:1, which the slurry showed no cracking or deformation when air dried, as well as no collapse and cracking after 900 C sintering. The optimized printing parameters for attapulgite-based ceramic slurry printing layer heights of 0.8 mm, the printing pressure of 0.10 MPa, and the printing speed at 20 mm/S. XRD confirmed that TiO_2 is a rutile phase. The stable and less active rutile phase of TiO_2 as a photocatalyst is confirmed by the inhibition zone test and growth inhibition assay. SEM results further showed agglomeration of TiO_2 after high-temperature sintering. This study lays a foundation for the attapulgite application in DSW printing to take advantage of its large specific surface areas.

Keywords: Nano TiO_2, 3D Printing, Ceramics Direct Slurry Writing DSW, Antibacterial, Mechanic Strengthening

1. Introduction

Compared with metals and polymers, ceramics have many advantages such as high melting point, high mechanical strength, and good thermal stability. The traditional preparation of ceramics is to mix all ingredients, mold them into shapes, and sinter at high temperatures. However, because the temperature of sintering ceramics is rather high (800 - 1200°C), there is little control over the size, shape, and desired performance of the final product. [1] Furthermore, the high brittleness of ceramics is another shortcoming of ceramic products. Despite these shortcomings and difficult manufacturing processes, ceramic is stable, non-toxic, strong oxidation-reduction and corrosion resistance to be studied for functional materials. For example, nano TiO2-based ceramics with antibacterial properties were investigated in the early '80s and TiO_2 has been widely recognized as an efficient photocatalyst. [2] As such, most studies of antibacterial ceramics focused on nano TiO_2 dopped photocatalytic materials. [3]

Ceramic 3D printing is a non-traditional additive manufacturing process based on the "discrete–stacking" principle that can shorten the production cycle, reduces production cost, and easy preparation of multifunctional, high-performance, and complex ceramic parts. It does not require a mold and can easily meet individual needs and

personalization. [4] In theory, it can realize the forming of ceramics with any complex structure. [5] Compared with traditional FDM and photolithography technology, ceramic materials have quite different viscosities and extrusion properties than those polymer materials. [6] To print ceramics, direct slurry writing DSW, also known as direct ink writing (DIW) technology was developed. By removing the heating and curing stages of FDM, the DSW technology has its advantages and challenges. For example, the ideal rheological properties of slurry can be achieved by the proper design of polymer side chain molecules [7] and the piston-assisted syringe method can be used to print the ceramic support at room temperature without thermal assistance. However, the slurry must be extruded smoothly through a narrow nozzle without clogging to form a continuous filament without collapsing or deformation. Without the heating element of FDM, the DSW-printed filament must be able to retain the shape and accurately follow the printing path. This would demand support during layer stacking to avoid the collapse of the 3D printing structure. [8]

Therefore, it is crucial to prepare ceramic slurry to be extrudable, shape-keeping, and self-supporting. [9] The prepared ceramic suspension determines the formation of ceramic suspension to manufacture solid ceramic components through injection molding. [10] The literature showed that, although the binder would assist the slurry preparation, it caused a large number of pores during the sintering process. This could lead to significant shrinkage or distortion in the final product. [11] Research and development of less toxic, environmentally friendly binders ceramic slurry to be used in the direct writing technology have been proposed. Chen *et al*. [12] successfully prepared TiO_2 ceramic slurry containing sodium hexametaphosphate and sodium alginate. Results showed that the ceramic slurry had good shear thinning behavior with 72 wt% TiO_2 content.

The combination of ceramic unique properties and DSW 3D printing technique prompt us to look into the attapulgite as a candidate for the ceramic slurry. Attapulgite soil is fine particle size, strong water absorption, and lightweight natural clay material that is an ideal reinforcing material for polymer materials. Especially, attapulgite clay has small shrinkage after drying and a large specific surface area due to its nanochannel structure, which is ideal for adsorption, decolorization, suspension, thixotropy, colloid, and ion exchange. It has a wide range of applications in petroleum, chemical, pharmaceutical, building materials, plastics, and other industries. In this study, various types of additives and binders will be added to TiO_2 and attapulgite slurry to investigate the impact on 3D printing. Particularly, PVP (polyvinyl pyrrolidone) and PEG (polyethylene glycol) will be used as binders will be added to the ceramic powders of attapulgite and TiO_2 mixture to serve as a precursor for manufacturing an antibacterial ceramic. The optimal binder ratio for ceramic slurries will be investigated by exploring the rheological properties of different mixtures of ceramic slurries, printing parameters, and drying and sintering conditions. The composition, morphology, geometric parameters, printing pressure, and printing speed will be optimized. Characterization tools such as XRD (diffraction of x-rays) and SEM will be used to show the microstructure of the 3D printing results. These results can shed some light on factors that influence the 3D printing quality and connection between the composite, 3D printing parameters, and the sintering process. This study can provide a foundation to further explore the unique property of attapulgite such as large specific surface areas.

2. Materials and Methods

2.1. Materials

Attapulgite and binder additive polyethylene glycol (PEG) were purchased from Yousuo Chemical Tech Company, Shangdong, China. Nano-TiO_2, agar, Sodium chloride, and binder additive polyvinyl pyrrolidone (PVP) were purchased from Chengdu Kelong Chemical Co., Ltd., Sichuan, China. Pryptone was purchased from Thermo Fisher Scientific Technologies. The beef extract was purchased from Beijing Aoboxing Biotechnology Co., Ltd.

2.2. Instruments & Characterization

All the 3D printings were carried out by 3D printer (model FSE-1) by Kunshan Bolimai 3D Printing Tech Co. Ltd. The drying of the 3D printing model was done in the muffle furnace (model DC–B8/13) by Shanghai Furnace Co. Ltd. The weighting was done on electric balance (model JJ-1000) by Changshu Measurement Instrument. Co. Ltd.

The surfaces of the 3DP model were imaged by scanning electron microscopy. All samples were fixed with double-sided carbon tape, and platinum sputter coating was performed with an SBC-12 ion sputterer (KYKY, Beijing, China) for 1 min. SEM images were then acquired using a VEGA 3 SBU (TESCAN, Czech) at 20 kV.

X-Ray structure analysis and determination of crystallinity of powder materials and 3DP tablets were performed using a DX-2600 X-Ray diffractometer (Fangyuan Instrument Co., Ltd., Dandong, China) with CuKα1 radiation and $\lambda = 1.5418$ Å. The intensity and voltage applied were 15 mA and 40 kV, respectively. The measurements were collected over a range of 2θ from 5° to 90° with a stepwise size of 0.05° at a speed of 5°/min. Scan to get the data and draw the X-ray diffraction pattern.

2.3. Printing Setup & Procedure

For consistency and easy comparison of printing results, this study adopted a simple square of 30 mm x 30 mm with a height of 5 mm printing model to test and optimize the printing parameters. This model was created in openCAD software and exported to STL file format, which was then sliced in cura software for printing. The following printing parameters were fixed or pre-defined with the 3D printer: the nozzle diameter is 1.55 mm, the flow rate is 200%, the printing temperature is 20°C, the filling density is 35%, and the filling pattern is a grid. As preliminary trials for the

feasibility test, three printing layer heights of 0.6, 0.8, and 1.0 mm, three piston pressures of 0.10, 0.15, and 0.20 MPa, and three printing speeds of 20, 30, and 40 mm/s were tested to optimize the respective parameters. After printing with DSW, compare the printing effect, and finally, determine the best printing parameters by evaluating the appearance and precision after printing.

2.4. Dry Sintering

The printed 3D structure was naturally dried at room temperature for 24 hours before it was heated in the muffle furnace up to 900°C with a heating rate of 5°C/min. The printed model structure would be maintained at 900°C for 2 hours. The final printing structure was cool to room temperature and measured for quality and comparison.

2.5. The Antibacterial Test

Gram-negative E. coli and gram-positive S. aureus bacteria were used in the inhibition zone test for the antibacterial property following the disc diffusion method. Take 2000 μL liquid culture medium, drop it into the lyophilized strain tube, shake slightly, and prepare the lyophilized strain into suspension. All the liquid is transferred into the test tube, placed on the shaking table, and cultured overnight. Take 2.50 g tryptone, 1.25 g beef extract, 1.50 g sodium chloride, 3.75 g agar, and a small amount of deionized water into the beaker. Put the beaker into the thermostatic electric heating jacket, transfer it into a conical flask after the beef paste is dissolved, and add water to 250 mL. Seal it and put it into the autoclave together with the culture dish for sterilization.

Dilute the cultured Escherichia coli into a bacterial suspension with a concentration of 104–105 cfu/mL. Pour the nutrient agar culture solution into the culture medium. After the culture medium is solidified, take 100μl of E. coli suspension onto the culture medium. Use the sterilized coating rod to evenly smear the bacterial solution and cover the dish. Use sterile tweezers to place the sample piece on the surface of the plate. After placing, gently press the sample piece to make it close to the surface of the plate. Place the culture dish under certain conditions for 24h and observe the results. Use the vernier caliper to measure the internal and external diameter difference (D–d) of the antibacterial ring. The width of the antibacterial ring is W=(D–d)/2. Take the average of the three measurements.

3. Results and Discussion

Without the heating and curing stages of FDM, the direct slurry writing (DSW) will be influenced greatly by the printing parameters and the quality of the ceramic slurry. Particularly, the viscosity of the slurry can vary greatly, which would require different piston pressure, the driving force to move the slurry from the cylinder to the printer nozzle. For materials with higher viscosity, lower pressure will cause a low shear rate at the nozzle when discharging, which will cause nozzle blockage. For materials with low viscosity, the slurry could flow out of the nozzle even without pressure. [13] Therefore, binders such as PVP (polyvinyl pyrrolidone) and PEG (polyethylene glycol) were used in this study to improve the control of flow and to improve the layer structure and binding efficiency. Furthermore, the printing layer height has a great influence on whether the slurry firmly adheres and the deposition time after discharging. [14] The printing speed is another important parameter, where the discharge of slurry should correlate well to the printing speed. When the speed is too fast and the slurry flow is lagging, the printing could break and a gap will show. When the speed is too slow, the slurry could stick to each other or clog the extrusion head. This will not affect the precision of the printing body, but also the printing quality. [15] Therefore, it is necessary to determine the suitable viscosity of the ceramic slurry for its printing feasibility.

3.1. DSW Printing Feasibility Test with PVP Binder

Since PVP was used as a binder while the amount of water will influence the viscosity of the ceramic slurry. The first DSW feasibility experiments were conducted with PVP and TiO_2 slurry. The amount of water to be used was first tested. While the amont PVP was maintained at 5% (w/W), the ratio TiO_2 and H_2O varies from 2:1, 2.5:1, 3:1, 3.5:1 and 4:1, respectively. As the ratio increases, the viscosity of the slurry also increases. Visual inspection demonstrated that the slurry batches with ratios of 2:1, 2.5:1, 3:1, and 3.5:1 were all well-mixed without obvious agglomeration or clumps. On the contrary, a slurry of TiO_2 to H_2O=4:1 ratio had too little water to dissolve all TiO_2 powder. Therefore, the slurry with a 4:1 ratio was not suitable for DSW printing. Interestingly, even though the slurry batches with the ratios of 2:1, 2.5:1, and 3:1 demonstrated shear thinning effects, after transferring the slurry to the compressing cylinder, their viscosities were a bit too low for any desirable DSW printing quality. Therefore, TiO_2 and H_2O ratio was maintained at 3.5:1 in the subsequent experiments.

Table 1. *The proportion of PVP and nano-TiO_2 slurry formula.*

Samples	PVP % (w/W)	Nano-TiO_2 % (w/W)	H_2O % (w/W)
1	0.00	77.78	22.22
2	5.00	73.89	21.11
3	10.00	70.00	20.00
4	15.00	66.11	18.89
5	20.00	62.22	17.78

By maintaining the TiO_2 and H_2O ratio at 3.5:1, the amount of PVP was adjusted from 0% (w/W) to 20% (w/W) as shown in Table 1. The slurry prepared with different concentrations of PVP demonstrated different printing results. For example, the slurry with 5% (w/W) PVP showed shear thinning behavior and had obvious non-Newtonian fluid characteristics. This was favorable for slurry extrusion from the nozzle, thus facilitating DSW printing. Meanwhile, the viscosity of the slurry decreases with the increase of PVP content. This is evidenced by the printing results shown in Figure 1 where (a) is 0% PVP content, (b) is 5% (w/W), (c) is 10% (w/W), and (d) is 15% (w/W) PVP content. One can see the deformation increases as PVP content increases. This might be due to the decreased distance between particles and

the interaction between the PVP binder and TiO_2 solid particles increases. As such, when the content of PVP reaches 20% (w/W), this batch was no longer suitable for DSW printing.

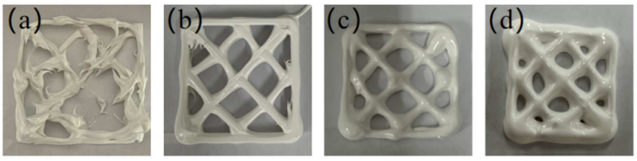

Figure 1. *DSW printing results of 0% (a), 5% (b), 10% (c), and 15% (d) (w/W) PVP content while maintaining the TiO_2:H_2O ratio at 3.5:1.*

One can see that the slurry with 0% (w/W) PVP content (Figure 1a) was unable to print a complete model. It seems the slurry has a high viscosity, which caused the drag of the moving nozzle. The model resulted in incomplete printing. The slurry batches with 5, 10, and 15% (w/W) PVP content (Figure 1b, 1c, & 1d) clearly showed increased liquidity and were able to print the complete model. This suggested the PVP could lower the viscosity of the slurry. However, batches with 10 & 15% (w/W) PVP content (Figure 1c & d) started showing the deformation of the final prints. This is due to the lower viscosity because of increased PVP content. Not surprisingly, the batch with 20% (w/W) PVP content (not shown) had the lowest viscosity and caused severe deformation, and resulted in the collapse during the drying and deposition stage. Therefore, batches with 10% (w/W) PVP content (Figure 1b) were selected as the optimal formula for the optimization of DSW printing parameters ceramic slurry.

Once the proper amount of TiO_2, H_2O, and binder ratio was determined, it would be used to optimize three printing parameters: the printing layer heights, the pressing pressure, and the printing speed. Based on the model and printer available, the following printing parameter ranges will be optimized: layer height 0.6–1.0 mm, pressure 0.1–0.2 MPa, speed 20–40 mm/s.

The printing layer heights optimization was carried out by fixing the printing pressure at 0.10 MPa and the printing speed at 20 mm/s. Three printing layer heights were tested at 0.6, 0.8, and 1.0 mm respectively. The printing quality was judged qualitatively based on the appearance of the integrity, deformation, collapse, and breakage of the final printing product. As shown in Table A1, the model cannot be printed completely when the layer height was set at 0.6 mm. When the layer height was set at 0.8 and 1.0 mm, the model can be printed completely. Due to the viscosity, all printouts showed some degree of collapse. Nevertheless, the printed model with 0.8 mm height has less deformation than the model with 1.0 mm layer height, and precision seems to be slightly better. Therefore, 0.8 mm was chosen as the preferred printing layer height for DSW printing.

A similar procedure was carried out to determine the pressure for the printing nozzle and the printing speed while holding the other printing parameters fixed. Table A2 showed that, while all pressures at 0.10, 0.15, and 0.20 MPa could print a complete model, the pressure of 0.20 MPa was determined to be the optimal nozzle pressure for DSW printing. Table A3 showed that at the set printing layer height of 0.8 mm and the printing pressure of 0.20 MPa, all printing speeds from 20–40 mm/s could produce decent printed models. To further quantitatively examine the quality of these trial prints, the average heights at the four corners of the printing models were collected and compared with the theoretical model heights. Figure 2 summarized these absolute errors of DSW printing results of the printing height (trial #1 not shown due to broken printout), the nozzle pressure (trials #4-6), and print speed 40 mm/s (trials #7-9). The results suggested that the printing height of 0.8 mm (trial numbers 2 &3), nozzle pressure of 0.20 MPa (trials #4-6), and print speed of 20 mm/s (trials #7-9) have the closest average heights at the four corners to that of the theoretical model. These printing parameters were consistent with previous qualitative assessments.

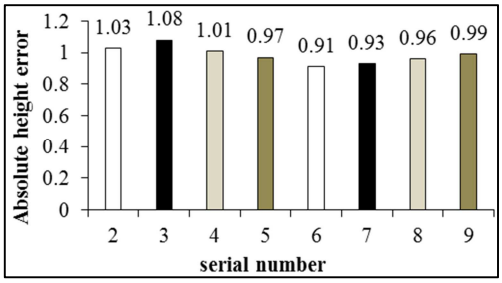

Figure 2. *The average heights at the four corners of the printing models when compared with the theoretical model heights.*

This combination of the PVP-TiO_2 formula and the optimal printing parameters is suitable for DSW printing. However, the deposition process seems still rough which caused round corners and collapse during the DSW printing. This could be due to (1) the size of the printing nozzle; (2) the viscosity might still be too high, causing the drag nonetheless; and (3) there is still shrinking and collapsing during the drying process, resulting in reduced precision. To investigate the effect of the sintering on the final printing model, all five models from Table 1 were printed using the optimal printing parameters identified aforementioned. These five models were sintered in a muffle furnace at 900°C after drying at room temperature for 24 hours. Models 1 - 3 appeared cracks after drying under room temperature and model 5 showed cracks after sintering. Only model 4 showed no apparent cracks, but a certain degree of shrinkage. Nonetheless, all models are dense ceramics with low compressive strength after sintering as shown in Table 2.

Table 2. *Pre-experiment of attapulgite/nano-TiO2.*

model	Printability	Self-supporting	Breakage	Change after sintering
1	×	–	–	–
2	×	×	–	–
3	√	×	√	More serious
4	√	√	×	Unchanged
5	×	–	–	–

3.2. DSW Printing Feasibility Test with PEG Binder

The DSW printing feasibility test was also carried out with a PEG binder similar to the PVP process as described in section 3.1. The formula of PEG ceramic slurry used in preparing the ceramic slurry was similar to those in Table 1 and shown in Table A4. Figure 3 showed the DSW printing results of (a) 0% PEG content, (b) 5% (w/W), (c) 10% (w/W), and (d) 15% (w/W) PEG content. Compared with PVP DSW printing results in Figure 1, one can see the deformation and collapse of PEG printing are more serious than the corresponding percentage of PVP. For example, the collapse in 15% (w/W) PEG content caused spacing to nearly vanished in the DSW printing. This indicates the PEG binder would lower the viscosity of the slurry. However, the quality of DSW printing with a PEG concentration of 5% seems to be better than that of a PVP binder.

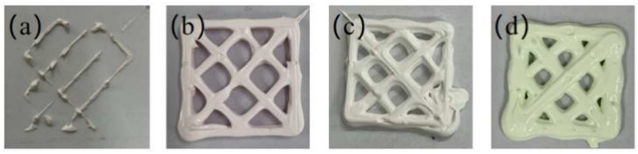

Figure 3. *DSW printing results of 0% (a), 5% (b), 10% (c), and 15% (d) (w/W) PEG content while maintaining the TiO_2:H_2O ratio at 3.5:1.*

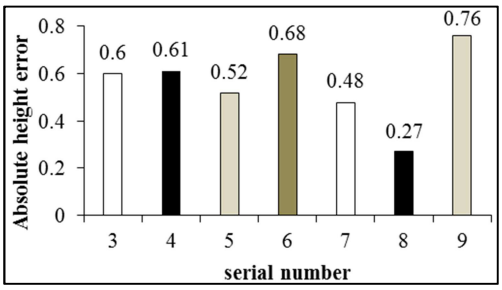

Figure 4. *The average heights at the four corners of the printing models when compared with the theoretical model heights.*

In the quantitative assessment of the DSW printing, Figure 4 shows the absolute error between the average heights at the four corners of the printing models and the theoretical model heights were all smaller than those of PVP as shown in Figure 3. The printing parameter optimization with 5%(w/W) PEG slurry showed that the printing layer heights (Table A5) at 1.0 mm, the printing pressure optimization (Table A6) at 0.15 MPa, and the printing speed (Table A7) all 20–40 mm/s could produce reasonable DSW printing. The quantitative examination of the printing quality using the average heights at the four corners of the printing models also suggested that these printing parameters produced the smallest absolute error as shown in Figure 4. Our assessment even suggests that DSW printing with PEG binder could achieve slightly better printouts than those with PVP binder. However, the slurry with PEG binder caused a serious deformation during the air drying at room temperature as Figures 3c & 3d depicted. This could be because the PEG binder facilitated TiO_2 particles to attract moisture from the air and further lowered the viscosity on the surface.

Furthermore, Table A8. Summary of PGE slurry samples 1-5 (Table A4) after sintering with these optimized printing parameters. After 24 hours of natural drying of ceramic bodies in each sample, the first three samples PEG samples 1-3 appeared cracks. Even though sample PEG–5 did not appear obvious cracks, the surface show pitted. This could be caused by the evaporation of a large amount of water during drying. All ceramic bodies showed some degree of shrinkage, curling, and warping. After sintering at 900°C in the muffle furnace, the cracking is more obvious. The dense ceramics were not formed as their compressive strength was small and brittle. Compared with the PVP binder, the overall performance of the PEG binder was poor, and did not significantly improve the rheological property of the slurry. Therefore, PEG was not considered in the following attapulgite slurry DSW printing.

3.3. DSW Printing Feasibility Test with Attapulgite Slurry

Apptpulgite is a crystalline magnesium aluminosilicate hydrate with active hydroxyl groups on the surface and zeolite-like channels inside. This unique structure renders a large specific surface area and is often used as an adsorbent, catalyst, and catalyst carrier. DSW printing technique could provide a new venue for its applications. [16] As shown in section 3.1, PVP binder could facilitate lower the viscosity of TiO_2 slurry that cause the deformation. A study showed that a small amount of attapulgite could effectively improve the thixotropic property and created an attraction force to form a stable microstructure and higher viscosity at rest. [17] Therefore, attapulgite is used to counter the viscosity deterioration caused by PVP binder to alleviate the viscosity, remedy the cracking and improve the compressive strength of ceramics. Three sets of PVP% were tested with the added attapulgite: group 1 of 10% (w/W) PVP and group 2 of 15% (w/W) PVP groups that both maintained PVP:attapulgite=1:1. A third group with 15% (w/W) PVP set PVP:attapulgite ratio at 1:1, 2:1, and 1:2. The specific proportion is summarized in Table 3.

Table 3. *Pre-experiment of attapulgite/nano-TiO2.*

sample groups	PVP % (w/W)	Attapulgite % (w/W)	TiO_2 % (w/W)	H_2O % (w/W)	Printability	Break
1-1	10.00	36.00	36.00	18.00	×	√
1-2	10.00	35.00	35.00	20.00	×	√
1-3	10.00	34.00	34.00	22.00	√	√
1-4	10.00	33.00	33.00	24.00	√	√
2-1	15.00	33.50	33.50	18.00	×	√
2-2	15.00	32.50	32.50	20.00	×	√
2-3	15.00	31.50	31.50	22.00	√	√
3-1	15.00	30.50	30.50	24.00	√	×
3-2	15.00	24.40	36.60	24.00	√	√
3-3	15.00	36.60	24.40	24.00	√	√

The printability was judged by integrity, deformation, and collapse. The experiment results showed that the cracks of the third group, especially sample 3-1, were relatively small compared with other samples. The DSW printing of the third group with the attapulgite is shown in Figure 5. The integrity of the DSW printing of this attapulgite group was improved over those of PVP or PEG alone. The number of printing layers without deformation or collapse is evidenced by the appearance of the printed wall as shown in Figure 5 (d). Adding attapulgite clearly could improve the viscosity of the ceramic slurry. The attapulgite/TiO_2: water ratio could be reduced from 3.5 to 2.5. The overall assessment suggests that the preferred attapulgite: TiO_2 ratio was 1:1 as shown in Figure 5 (attapulgite sample 3-1 in Table 3), which showed less deformation or defects.

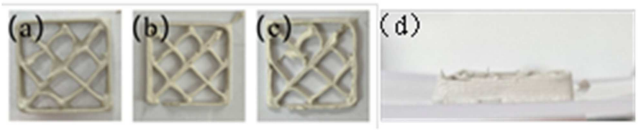

Figure 4. *DSW printing results of 0% (a), 5% (b), 10% (c), and 15% (d) (w/W) PEG content while maintaining the TiO_2:H_2O ratio at 3.*

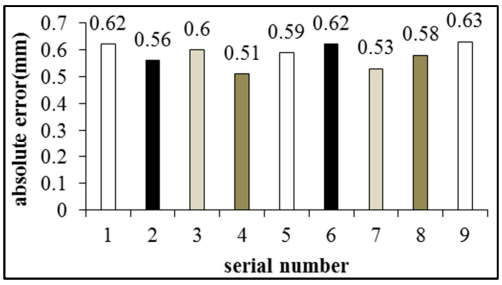

Figure 5. *DSW printing results of 0% (a), 5% (b), 10% (c), and 15% (d) (w/W) PEG content while maintaining the TiO_2:H_2O ratio at 3.5.*

Following the same procedure and quality assessment protocol, the printing parameters could be optimized using the attapulgite sample 3–1. As shown in Table A9, all printing layer heights 0.6-1.0 mm could be printed with integrity and no deformation, collapse, or breakage were observed. This was a drastic difference that those with PVP- or PEG-only samples. The same integrity was also observed with the printing pressure (Table A10) and the printing speed (Table A11) to produce reasonable DSW printouts. The quantitative examination of the printing quality using the average heights at the four corners of the printouts (Figure 5) suggested that printing layer heights of 0.8 mm, the printing pressure of 0.10 MPa, and the printing speed at 20 mm/S be the optimal DSW printing parameter with attapulgite ceramic slurry. At this set of DSW printing parameters, the printouts had the smallest absolute error of 0.56 mm, 0.51 mm, and 0.53 mm, respectively.

Compared with the PVP-or PEG-added ceramic slurries, the viscosity of these attapulgite models was more suitable for DSW printing. The thixotropic property enhancement by the added attapulgite did improve the rheological appearance such as the shape of the final product, shrinkage-caused cracking, and the surface. With added attapulgite, the structure was small and net with no obvious breakage or deformation, and the surface is smooth, which can maintain a good shape over a long period without cracking.

The DSW printings of attapulgite model 3-1, 3-2, and 3-3 were also sintered in a muffle furnace at 900°C for two hours after room temperature drying for 24 hours. Results showed that there was no obvious shrinkage or cracking occurred in all three models. However, none of them formed dense ceramics with low compressive strength. Table 4 summarizes the printability and other properties of the attapulgite-added ceramic slurry.

Table 4. *Quality of attapulgite-based ceramic paste after sintering.*

samples	Printability	Self-supporting	Breakage	Change after sintering
3–1	√	×	√	No change
3–2	√	×	√	No change
3–3	√	×	√	No change

3.4. XRD Results

Sintering is the high-temperature heat treatment of the ceramic body. The particles in the ceramic migrate, shrink, and grow. The pores are removed to obtain a dense polycrystalline ceramic material. Here, the attapulgite-based sample 3-2 before and after sintering were examined by XRD characterization, and the results are shown in Figure 6, labeled as a (top red color) and b (middle blue color), respectively. A standard XRD spectrum of TiO_2 from JADE software was listed in black at the bottom as a comparison. One can see that 2θ peaks at 25.3°, 27.5°, and 30.8° are the strongest characteristic peaks of anatase, rutile, and brookite, respectively. It is found that the nano TiO_2 is in the rutile phase before sintering. The diffraction peaks are not sharp, which suggests that the degree of crystallization is poor. The grains of nano TiO_2 increased after sintering.

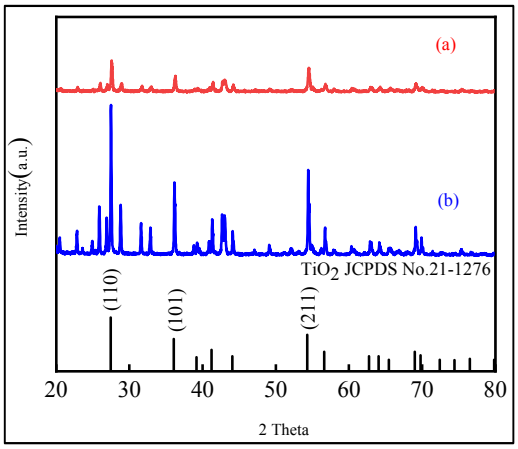

Figure 6. *The XRD characterization of attapulgite-based sample 3-2 before (a) top red color, after sintering (b) middle blue color, and standard TiO2 (c) bottom black color.*

3.5. SEM Results

As a comparison, the SEM results of attapulgite-based

DSW printing (a: before sintering and b: after sintering) and PVP-based DSW printing (c: before sintering and d: after sintering) are shown in Figure 7. The TiO_2 microstructure is a small sphere structure with a smooth surface. When it is not sintered, TiO_2 agglomerates and attaches to PVP (Figure 7c). When PVP is decomposed after high-temperature sintering, TiO_2 is left and distributed (Figure 7d). The grain size of TiO_2 grew due to the aggregation after sintering. The attapulgite-based ceramic printout, on the other hand, showed no obvious change in morphology except the grain size also increased after sintering. TiO_2 is agglomerated on the attapulgite before and after sintering.

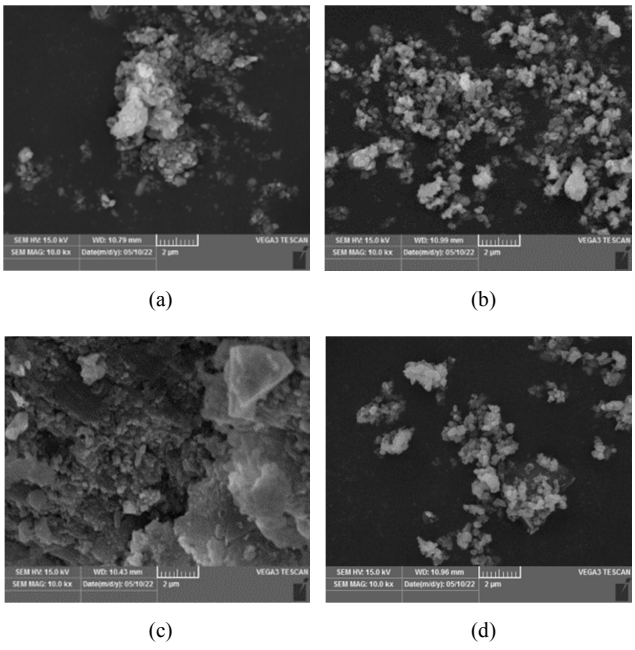

(a) (b)

(c) (d)

Figure 7. *The XRD characterization of attapulgite-based sample 3-2 before (a) top red color, after sintering (b) middle blue color, and standard TiO2 (c) bottom black color.*

3.6. SEM Results

A study showed [18] that TiO_2 demonstrates an antibacterial effect only when it is exposed to light with a wavelength of 387.5 nm or less. In this study, UV lights at 254 nm, 365 nm, and natural light were used for 24 hours respectively to observe the antibacterial property by the inhibition zone test. Results showed that there was no bacteriostatic circle on each group of samples under 254 nm UV light or under natural light irradiation. Under 365 nm irradiation, only the attapulgite-based sample 3-2 demonstrated a small bacteriostatic circle in group b (within the margin of error). According to the previous XRD spectra, the nano TiO_2 is in the rutile phase before and after sintering. Rutile is in a stable state relative to anatase, so the activation performance of anatase for photocatalysis is stronger than that of rutile. This might be the reason for the failure to demonstrate antibacterial properties with this batch of the sample with the nano TiO_2.

4. Conclusions

The stable, non-toxic, strong oxidation-reduction and corrosion-resistance properties of ceramics have been widely studied as a functional material. In this study, TiO_2 ceramic slurries with PVP binder, PEG binder, and attapulgite were prepared. The formula and DSW printing parameters were strategically and thoroughly optimized. The DSW printability and feasibility were evaluated by both qualitative assessments via integrity, deformation, collapse, and breakage indicators and quantitative assessment using the absolute error between the average heights at the four corners of the printing models and the theoretical model heights. The rheological and thixotropic properties of these different ceramic slurries were compared. The printability of TiO_2 ceramic slurry increases from PVP-, attapulgite-, and PEG-based slurry in terms of absolute error. The printouts of PEG slurry are visually better than PVP-based slurry. However, the shear thinning behavior of PEG-based slurry becomes more serious and viscosity decreases to create a collapse of the printout. The results show that 10% PVP and 5% PEG ceramic slurry were suitable for DSW printing. The optimized printing parameters for PVP-based slurry are a printing layer height of 0.8 mm, printing pressure of 0.20 MPa, and printing speed of 20 mm/s, respectively; for PEG-based slurry is a printing layer height of 1.0 mm, printing pressure of 0.15 MPa, and printing speed of 30 mm/s, respectively; and attapulgite-based ceramic slurry printing layer heights of 0.8 mm, the printing pressure of 0.10 MPa, and the printing speed at 20 mm/S. Under this printing parameter, the customized direct writing molding technology can make the slurry extrude smoothly. XRD results confirmed TiO_2 as a rutile phase and do not produce antibacterial property. The SEM results showed that TiO_2 agglomerates were on the binder and attapulgite surface before sintering. The TiO_2 grain size increased significantly after high-temperature sintering and uniformly distributed after binders burnt away. In this study, we have successfully manufactured attapulgite ceramics through DSW printing and optimized the formulation and 3DP process conditions. This study revealed a generalized optimization protocol and procedure that could be applied to in preparing and manufacturing of parts with fine and complex three-dimensional architecture under a mild condition, particularly of advanced ceramic preparation. The future research areas include tissue engineering, microelectronics, wearable gears, arts and designs, aerospace and defense applications.

Acknowledgements

HJSF would like to acknowledge the partial financial support from the Science Foundation of Sichuan University of Science & Engineering (2020RC06) and the Natural Science Foundation of Sichuan Province (SYZ202133 & 2022JDGD0041). The authors would like to thank the College of Chemical Engineering at Sichuan University of Science and Engineering for providing the lab facility and

logistic support for this project.

Appendix

Table A1. *Effect of printing layer height at 0.6, 0.8 and 1.0 mm with PVP slurry.*

Parameter	1	2	3
Height/mm	0.6	0.8	1.0
Pressure/MPa	0.10	0.10	0.10
Speed/mm · s^{-1}	20	20	20
Integrity	×	√	√
Deformation	×	×	×
Collapse	√	√	√
Break	×	×	×

Table A2. *Effect of pressure for the printing nozzle at 0.10, 0.15, and 0.20 MPa with PVP slurry.*

Parameter	4	5	6
Height/mm	0.8	0.8	0.8
Pressure/MPa	0.10	0.15	0.20
Speed/mm · s^{-1}	20	20	20
Integrity	×	√	√
Deformation	×	×	×
Collapse	√	√	√
Break	×	×	×

Table A3. *Effect of printing speed at 20, 30, and 40 mm/s with PVP slurry.*

Parameter	7	8	9
Height/mm	0.8	0.8	0.8
Pressure/MPa	0.20	0.20	0.20
speed/mm · s^{-1}	20	30	40
Integrity	√	√	√
Deformation	×	×	×
Collapse	√	√	√
Break	×	×	×

Table A4. *Formula trials of PEG added nano-TiO_2 slurry.*

Samples	PEG %(w/W)	Nano-TiO_2 %(w/W)	H_2O %(w/W)
PEG–1	0.00	77.78	22.22
PEG–2	5.00	73.89	21.11
PEG–3	10.00	70.00	20.00
PEG–4	15.00	66.11	18.89
PEG–5	20.00	62.22	17.78

Table A5. *The DSW printing parameter optimization of printing layer height with PEG slurry.*

Parameter	1	2	3
Height/mm	0.6	0.8	1.0
Pressure/MPa	0.10	0.10	0.10
Speed/mm · s^{-1}	20	20	20
Integrity	×	×	√
Deformation	×	×	×
Collapse	×	×	×
Break	√	√	√

Table A6. *The DSW printing parameter optimization of printing pressure with PEG slurry.*

Parameter	4	5	6
Height/mm	1.0	1.0	1.0
Pressure/MPa	0.10	0.15	0.20
Speed/mm · s^{-1}	20	20	20
Integrity	√	√	√
Deformation	×	×	×
Collapse	×	×	√
Break	√	×	×

Table A7. *The DSW printing parameter optimization of printing speed with PEG slurry.*

Parameter	7	8	9
Height/mm	1.0	1.0	1.0
Pressure/MPa	0.15	0.15	0.15
Speed/mm · s^{-1}	20	30	40
Integrity	√	√	√
Deformation	×	×	×
Collapse	×	×	×
Break	×	×	×

Table A8. *Summary of PGE slurry samples 1-5 after sintering.*

Samples	Printability	Self-supporting	Best print parameters	Break	Change after sintering
PEG-1	×	–	–	–	–
PEG-2	×	–	–	–	–
PEG-3	√	×	1.0 mm, 0.15 MPa, 30 mm · s^{-1}	√	More serious
PEG-4	√	√	1.0 mm, 0.10 MPa, 40 mm · s^{-1}	√	More serious
PEG-5	×	√	–	√	No change

Table A9. *The DSW printing parameter optimization of printing layer height with attapulgite slurry.*

Parameters	1	2	3
Height/mm	0.6	0.8	1.0
Pressure/MPa	0.10	0.10	0.10
Speed/mm ·s^{-1}	20	20	20
Integrity	√	√	√
Deformation	×	×	×
Collapse	×	×	×
Break	×	×	×

Table A10. *The DSW printing parameter optimization of printing pressure with attapulgite slurry.*

Parameters	4	5	6
Height/mm	0.8	0.8	0.8
Pressure/MPa	0.10	0.15	0.20
Speed/mm · s^{-1}	20	20	20
Integrity	√	√	√
Deformation	×	×	×
Collapse	×	√	√
Break	×	×	×

Table A11. *The DSW printing parameter optimization of printing speed with attapulgite slurry.*

Parameters	7	8	9
Height/mm	0.8	0.8	0.8
Pressure/MPa	0.10	0.10	0.10
Speed/mm · s^{-1}	20	30	40
Integrity	√	√	√
Deformation	×	×	×
Collapse	×	√	√
Break	×	×	×

References

[1] Dhainaut J, Bonneau M, Ueoka R et al. (2020). Formulation of Metal-Organic Framework Inks for the 3D Printing of Robust Microporous Solids toward High-Pressure Gas Storage and Separation. ACS Appl Mater Interfaces. 12 (9), 10983-10992, doi: 10.1021/acsami.9b22257.

[2] Jiang Y, Zhao W, Li S, et al. (2022). Elevating Photooxidation of Methane to Formaldehyde via TiO(2) Crystal Phase Engineering. J Am Chem Soc. 144 (35), 15977-15987, doi: 10.1021/jacs.2c04884.

[3] Ye M, Gong J, Lai Y, et al. (2012). High-efficiency photoelectrocatalytic hydrogen generation enabled by palladium quantum dots-sensitized TiO2 nanotube arrays. J Am Chem Soc. 2012. 134 (38), 15720-3, doi: 10.1021/ja307449z.

[4] Ligon SC, Liska R, Stampfl J, et al. (2017). Polymers for 3D Printing and Customized Additive Manufacturing. Chem Rev. 117 (15), 10212-10290, doi: 10.1021/acs.chemrev.7b00074.

[5] Wang P, Li J, Wang G, et al. (2022). Selectively Metalizable Low-Temperature Cofired Ceramic for Three-Dimensional Electronics via Hybrid Additive Manufacturing. ACS Appl Mater Interfaces. 14 (24), 28060-28073, doi: 10.1021/acsami.2c03208.

[6] Mahmoudi M, Wang C, Moreno S, et al. (2020). Three-Dimensional Printing of Ceramics through "Carving" a Gel and "Filling in" the Precursor Polymer. ACS Appl Mater Interfaces. 12 (28), 31984-31991, doi: 10.1021/acsami.0c08260.

[7] Ho CMB, Ng SH, and Yoon YJ (2015). A review on 3D printed bioimplants. International Journal of Precision Engineering and Manufacturing. 16 (5), 1035-1046.

[8] Yao B, Xu Z, Liu J, et al., Design a Viable 3DP Processing for Producing Effective Controlled-Release Pesticide. American Journal of Science, Engineering and Technology, 2023 (in press).

[9] Yoon K, Han J, Choi B, et al. (2018). Three Dimensional Printed Poly vinyl alcohol Substrate with Controlled On Demand Degradation for Transient Electronics. ACS Nano. 12 (6), 6006-6012. doi: 10.1021/acsnano.8b02244.

[10] Bagheri A, Bainbridge CWA, Engel KE, et al. (2020). Oxygen Tolerant PET-RAFT Facilitated 3D Printing of Polymeric Materials under Visible LEDs. ACS Applied Polymer Materials. 2 (2), 782-790, doi: 10.1021/acsapm.9b01076.

[11] Waheed S, Cabot JM, Smejkal P, et al. (2019). Three-Dimensional Printing of Abrasive, Hard, and Thermally Conductive Synthetic Microdiamond-Polymer Composite Using Low-Cost Fused Deposition Modeling Printer. ACS Appl Mater Interfaces. 11 (4), 4353-4363, doi: 10.1021/acsami.8b18232.

[12] Chen T, Xiao H, and Shannon R (2019). Does dual-energy computed tomography pulmonary angiography (CTPA) have improved image quality over routine single-energy CTPA? J Med Imaging Radiat Oncol. 63 (2), 170-174, doi: 10.1111/1754-9485.12845.

[13] Tully JJ and Meloni GN (2020), A Scientist's Guide to Buying a 3D Printer: How to Choose the Right Printer for Your Laboratory. Anal Chem. 92 (22), 14853-14860, doi: 10.1021/acs.analchem.0c03299.

[14] Tucker LH, Conde-Gonzalez A, Cobice D, et al. (2018). MALDI Matrix Application Utilizing a Modified 3D Printer for Accessible High Resolution Mass Spectrometry Imaging. Anal Chem. 90 (15), 8742-8749, doi: 10.1021/acs.analchem.8b00670.

[15] Anciaux SK, Geiger M, and Bowser MT (2016), 3D Printed Micro Free-Flow Electrophoresis Device. Anal Chem. 88 (15), 7675-82, doi: 10.1021/acs.analchem.6b01573.

[16] Xue G (2021). TechnoIogy Progress of Dyeing Wastewater Treatment. Ind. Water Treat. 41 (9), 10–17. doi: 10.19965/j.cnki.iwt.2021-0433.

[17] Panda BN, Ruan SQ, Unluer C, et al. (2018). Improving the 3D printability of high volume fly ash mixtures via the use of nano attapulgite clay. Composites Part B: Engineering, 165, 75-83, doi: 10.1016/J.COMPOSITESB.2018.11.109.

[18] Chen H, Zhang J, Yang F, et al. (2022). Implanting a Copper Ion into a TiO_2 Nanorod Array for the Investigation on the Synergistic Antibacterial Mechanism between Mechanical Cracking and Chemical Damage. ACS Biomater. Sci. Eng. 8 (4), 1464–1475, DOI: 10.1021/acsbiomaterials.2c00089.